ELSEVIER

Contents lists available at ScienceDirect

Electrochimica Acta

journal homepage: www.elsevier.com/locate/electacta



Tuning electrochemical performance of carbon-sphere-based supercapacitors by compressive stress



Wei Sun^{a,b}, Yulin Zhang^b, Fuqian Yang^{b,*}

- ^a College of Chemistry, Chemical Engineering and Environmental Engineering, Liaoning Shihua University, Fushun, Liaoning, 113001, China
- b Materials Program, Department of Chemical and Materials Engineering, University of Kentucky, Lexington, KY 40506, United States

ARTICLE INFO

Article history: Received 21 February 2020 Revised 9 July 2020 Accepted 2 August 2020 Available online 5 August 2020

Keywords: Supercapacitor Compression Capacitance Ir drop Nominal diffusivity

ABSTRACT

The progress in flexible/stretchable electronics has increased the demand to develop highly reliable and efficient devices and systems for energy storage, which likely experience large mechanical stresses/deformation. In this work, we systematically investigate the effects of compressive stress on the electrochemical performance of symmetrical supercapacitor cells with xylose-derived activated-carbon spheres as electrode materials under different current densities. The electrolytes are aqueous solutions with different Na₂SO₄ concentrations; the compressive stress is in a range of 2.55 to 40.75 MPa. Increasing the compressive stress from 2.55 to 40.75 MPa leads to the increase of the specific gravimetric capacitance from 123.6 to 238.1 F g^{-1} under a current density of 1 A g^{-1} and the decrease of IR drop from 0.18 to 0.04 V. A power-law relationship between the specific gravimetric capacitance and the compressive stress is derived under the framework of mechanical deformation. This relationship is qualitatively in accord with the experimental results. There exists stress-assisted diffusion of ions in the activated carbon spheres during electrochemical cycling, and the nominal diffusion coefficient of ions in the activated carbon spheres is an exponential function of the compressive stress. The results reveal that increasing the compaction of activated carbon can increase the charge storage in supercapacitors.

© 2020 Elsevier Ltd. All rights reserved.

1. Introduction

The progress in flexible/stretchable electronics has attracted great interest to develop flexible/stretchable devices and systems for energy storage [1–3] in order to meet the energy/power requirements. Both metal-ion batteries (MIBs) and supercapacitors have exhibited potential as energy-storage devices for flexible/stretchable electronics. However, supercapacitors with high power density, fast charge/discharge rates and long-lasting cycle life [4–6] have superior advantages over MIBs, including lithiumion batteries, for the applications in power electronics, power systems [7] and hybrid electric vehicles, which require rapid power supply and energy recovery [3,8].

The successful application of supercapacitors in flexible/stretchable electronics requires the understanding of the effects of mechanical deformation on the electrochemical performance of supercapacitors. Li et al. [3] studied the electrochemical behavior of carbon-nanotube-based supercapacitors under compression and observed the increase of gravimetric capacitance with pressure for the pressure up to ~40 kPa for the electrolytes

of LiOH, NaOH and KOH. Further increasing pressure did not cause any significant change in the gravimetric capacitances for the supercapacitors. Gourdin et al. [9] investigated the effect of stacking pressure on the capacitance of the supercapacitors with organic electrolyte of 1 M tetraethylammonium tetrafluoroborate and activated carbons (ACs) as electrode materials. They claimed that the pressure had a limited effect on the capacitance of the supercapacitors. Li et al. [10] examined the pressure effect on the gravimetric capacitance and electrochemical impedance of the supercapacitors with ACs as electrode materials and Na2SO4 as electrolyte. They observed that increasing force in the range of 0 to 800 N led to the increase of the gravimetric capacitance from 19.34 F/g to 44.87 F/g and the decrease of electrochemical series resistance (ESR) from ~11 Ω to ~1 Ω and increasing the electrolyte concentration led to the decrease of the electrochemical serial resistance. Masarapu et al. [11] investigated the pressure effect on the electrochemical performance of flexible supercapacitors with nanostructured AC fibers as electrode materials in the systems for various electrolytes, including KOH, NaOH, LiOH, KCl and LiCl. They found that the gravimetric capacitance first increased slowly, then increased rapidly and finally reached plateau with increasing the pressure for all the electrolytes. Zhang et al. [12] assembled symmetric stripe-like supercapacitors cells with two AC-coated

^{*} Corresponding author.

E-mail address: fyang2@uky.edu (F. Yang).

steel stripes as electrodes and tetrabutylammonium tetrafluoroborate as electrolyte, and studied the electrochemical performances of the supercapacitors under three tensile loads of 0, 100 and 200 N and three compressive loads of 0, 7.2 and 8.9 N. They found that the capacitance under 200 N is less than that under 100 N and increasing the compressive load led to slight increase in the capacitance. Jia et al. [13] revealed the strain dependence of the electrochemistry of deformable supercapacitors with electrode material from polyaniline and electrolyte from polymer hydrogel. They demonstrated that increasing the stretch to 600% increased the capacitance retention to 162%. They attributed such behavior to the reduction of the distance for ionic migration due to the increase in the contact between the CNT paper and the PANI electrode and the thickness decrease of hydrogel. However, they found that compression had limited effect. In general, all these studies have revealed the potential effects of mechanical load/deformation and electrolyte concentration on the electrochemical behavior of supercapacitors. However, few studies have addressed the effects of electrolyte concentration and pressure on ionic diffusion, which plays an important role in determining the electrochemical performance of supercapacitors, and there are few theoretical analyses available in literature.

Considering the wide use of ACs in supercapacitors and the possible synthesis of ACs from sustainable biomass and biowastes, we study the electrochemical performance of symmetrical supercapacitors with AC spheres as electrode material under mechanical compression. The AC spheres are made from xylose (98%, Reagent) via hydrothermal carbonization and chemical activation. The study is focused on the effects of pressure and electrolyte concentration on the electrochemical capacitance and ionic diffusion in the AC spheres during electrochemical cycling. A simple relationship between the specific gravimetric capacitance and the compressive stress, which takes into account the effect of porosity, is derived under the framework of mechanical deformation. Such an approach is different from the work by Masarapu et al. [11], whose analysis was based on the initial topology of current collectors. The stress-assisted diffusion of ions during electrochemical cycling is revealed.

2. Experimental details

2.1. Synthesis of AC spheres

Following the method given by Sun et al. [14], we prepared AC spheres from the aqueous solution of xylose (98%, Reagent). Briefly, hydrothermal carbonization of the aqueous solution of xylose (20 wt% in concentration) was performed in a sealed Teflonlined-stainless-steel autoclave in an oven at 180 °C for 24 hrs. The solid product collected from the hydrothermal carbonization was washed first for 5 times with deionized water and dried then in a vacuum oven at 80 °C for 24 h. Further carbonization of the solid product was conducted at 500 °C for 2 hrs in a tube furnace (OTF-1200X, HF-Kejing) under nitrogen environment to improve structural stability of carbonized materials. The carbonized materials were chemically activated at 800 °C for 1 hrs under nitrogen environment. The chemical agent was KOH, and the mass ratio of KOH to the carbonized materials was 1:3. The chemically activated carbons were washed with sulfuric acid for 5 times, rinsed then with deionized water, and dried finally in a vacuum oven at 80 °C for 24 hrs.

2.2. Characterizations of AC spheres

The morphology of the chemically activated carbons was analyzed on a scanning electron microscope (SEM) (Hitachi S-4800, Japan) and a transmission electron microscope (TEM) (JEM-2100F,

Japan), and the surface characterization of the chemically activated carbons was analyzed by physisorption (Micromeritics surface characterization, USA). We used the density functional theory (DFT) to calculate the surface area, total pore volume and porewidth distribution of the chemically activated carbons, respectively, from the nitrogen adsorption/desorption isotherms, which were curve-fitted by the cylindrical-pore-QSDFT model. The calculation of the total pore volume was based on the amount of N2 gas adsorbed at a relative pressure of 0.99. S_{micro} (V_{micro}) represents the fraction of the cumulative surface area (pore volume) of the pores with width in a range of 0-2 nm, and S_{meso} (V_{meso}) represents the fraction of the cumulative surface area (pore volume) of the pores with width in a range of 2-50 nm. The microstructure and chemical bonding of the chemically activated carbons were characterized, respectively, on an X-ray power diffractometer (D8 Advance, Germany) and a Raman spectrometer (DXR, Thermo Fisher, USA).

2.3. Electrochemical characterization of symmetric supercapacitor cells

Symmetric supercapacitor cells were assembled with two stainless-steel cylinders as current collectors, a fiberglass paper (VWR 96, UK) as separator and aqueous solution of Na₂SO₄ (≥ 99.5%, Reagent) as electrolyte. The concentration of Na₂SO₄ in aqueous electrolyte varied in a range of 0.125 to 1 M. Electrodes in the shape of disc with ~5 mm in diameter and ~0.1 mm in thickness were prepared. The electrode materials consisted of the chemically activated carbons and Teflon powder with a ratio of 9:1, and the loading mass was 8 mg per electrode. The electrochemical performance of the symmetric supercapacitor cells, including cyclic voltammetry (CV), galvanostatic charge-discharge (GCD) tests and electrochemical impedance (EIS), was investigated on an electrochemical workstation (PARSTAT MC Princeton Applied Research, USA) under compressive loads of 50, 100, 200, 400 and 800 N, respectively, corresponding to compressive stresses of 2.55, 5.09, 10.19, 20.38 and 40.75 MPa. Note that each supercapacitor cell was used only for a set of tests (CV, GCD and EIS). The experimental setup is schematically illustrated in Illustration 1.

The specific gravimetric capacitance per electrode of a symmetrical supercapacitor cell is calculated from a GCD curve as

$$C = \frac{2I}{m} (\frac{dV}{dt})^{-1} \tag{1}$$

where I is the current intensity passing through the supercapacitor cell, m is the total mass of the AC spheres used in the supercapacitor cell (m/2 is the mass per electrode), and dV/dt is the "average" slope of the line segment of the discharge phase after the IR drop. The series resistance, R_S , is determined from the left intercept of the Nyquist plots with the z' axis.

3. Results

Fig. 1a shows a SEM image of the chemically activated carbon particles. All the AC particles are presented in the shape of nearly perfect sphere. This result suggests that the processes used in this work are able to produce AC spheres, even though the chemical activation with the agent of KOH was used. The size distribution of the AC spheres is depicted in Fig. 1b. The size of the AC spheres varies in a range of 0.55 to 1.15 μ m, and the average size is 0.86 \pm 0.13 μ m.

Fig. 1c shows a TEM image of the AC spheres. In general, the surfaces of the AC spheres are "smooth". The HRTEM (high-resolution TEM) image of an AC sphere shown in Fig. 1d reveals amorphous structure of the AC spheres.

Fig. 2a shows the XRD pattern of the AC spheres. There are two broad diffraction peaks at 2θ being ~20.0° and 43.1° The

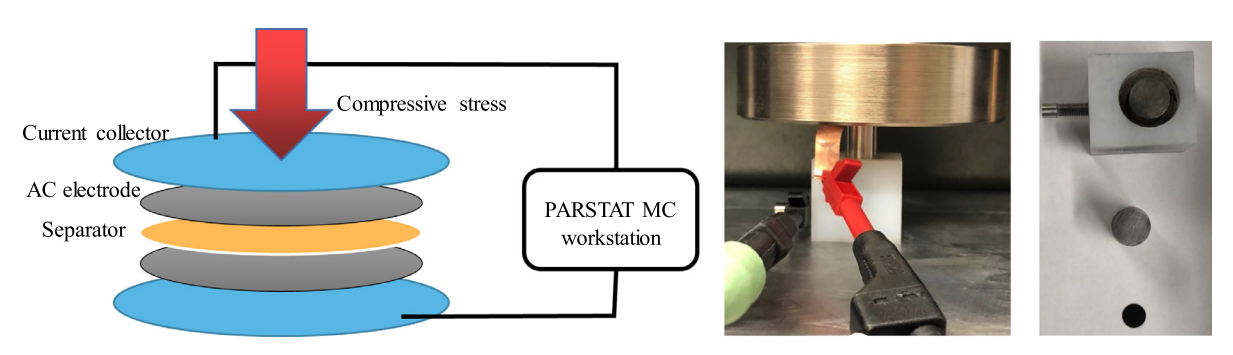


Illustration 1. Optical images of experimental setup.

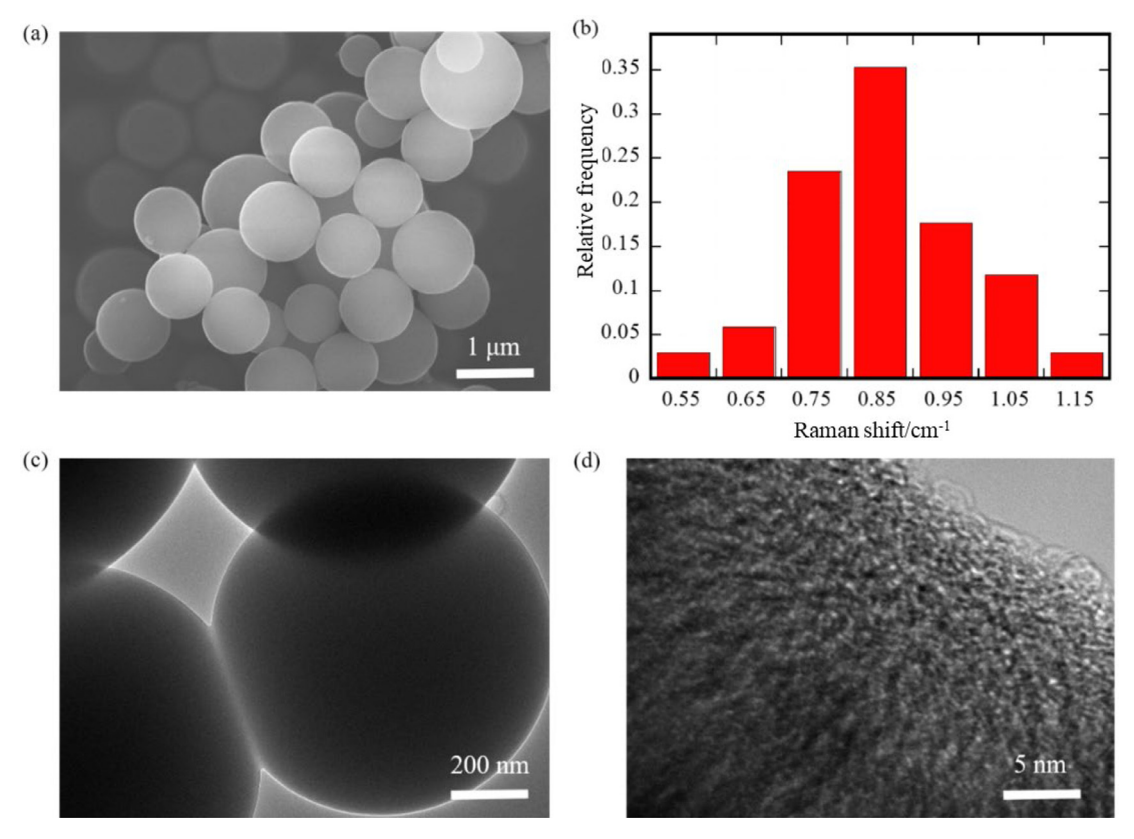


Fig. 1. (a) SEM image of the chemically activated carbon particles, (b) size distribution of the AC spheres, (c) TEM image of the AC spheres, and (d) HRTEM of an ACS sphere.

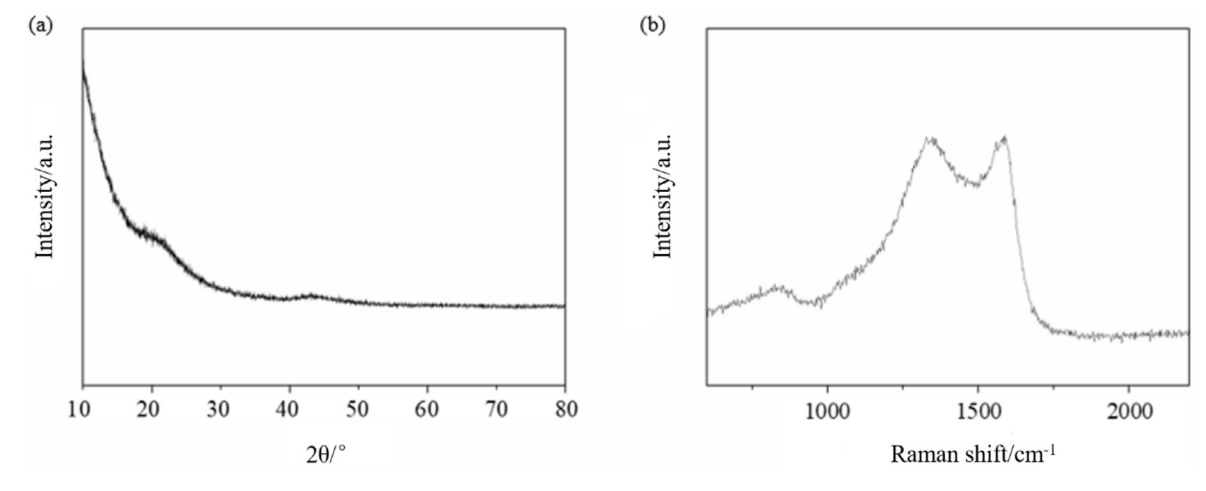


Fig. 2. XRD pattern (a) and Raman spectrum (b) of the AC spheres.

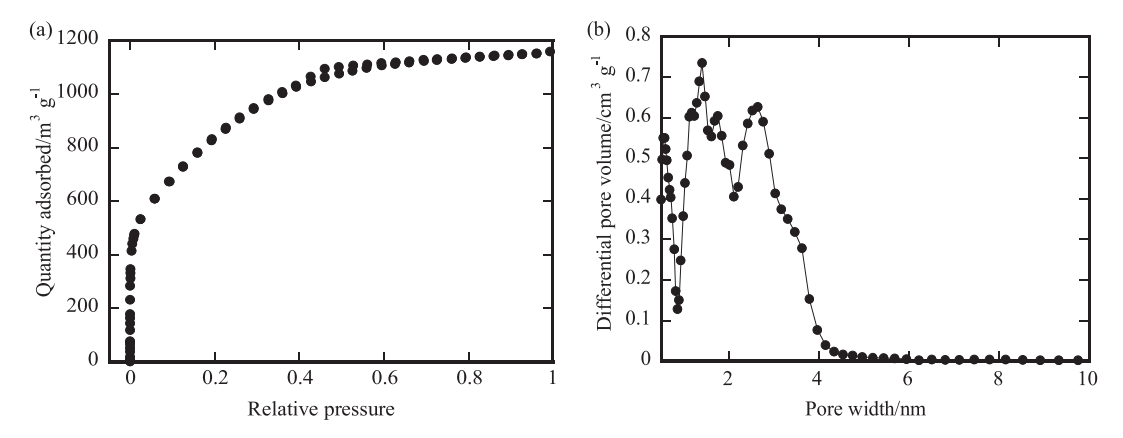


Fig. 3. (a) Nitrogen adsorption/desorption isotherms, and (b) distribution of pore widths.

Table 1Surface properties of the AC spheres.

$S_{DFT}/m^2 \ g^{-1}$	V _{tot} /cm ³ g ⁻¹	S _{micro} /%	S _{meso} /%	V _{micro} /%	V _{meso} /%
2675	1.625	72.5	27.5	49.9	50.1

broad diffraction peaks confirm the amorphous structure of the AC spheres with limited crystallinity. The chemical activation of the xylose-derived carbonized product with KOH at 800 °C for 1 h did not cause significant graphitization, which is qualitatively in agreement with the results reported in literature [15,16]. The Raman spectrum of the AC spheres shown in Fig. 2b reveals the presence of two typical peaks around 1345 cm⁻¹ and 1587 cm⁻¹, corresponding to the D band (representing defects and disorders [17]) and the G band (representing the $\rm E_{2g}$ mode of 2D graphite [18]), respectively. The intensity ratio of the D-band to the G-band ($\rm I_D/I_G$) is 0.98, supporting the low crystallinity (graphitization) of the AC spheres in good agreement with the XRD pattern.

The nitrogen adsorption/desorption isotherms of the AC spheres are presented in Fig. 3a. According to the IUPAC classification [19], the nitrogen adsorption/desorption isotherms of the AC spheres follow a mixed mode. The rapid increase in the adsorption at small relative pressure is attributed to the monolayer adsorption on the surfaces of the micropores [20]. Increasing the relative pressure led to the change of the isotherm from the monolayer adsorption to the Type IV mode with the characteristic of mesopores. The hysteresis loop in the nitrogen adsorption/desorption isotherms also points to the presence of the mesopores in the AC spheres.

Using the nitrogen adsorption/desorption isotherms in Fig. 3a, we obtain the distribution of the pore widths of the AC spheres (Fig. 3b). There is a broad distribution of the pore widths, consisting of micropores and mesopores. The cutoff pore width is ~4 nm. Table 1 summaries the surface properties of the AC spheres, in which "S" represents surface area, and "V" represents volume. Note that the gravimetric DFT-surface area of the AC spheres is ~2675 m^2/g .

Fig. 4a shows the CV curves of the symmetrical supercapacitor cells with the electrolyte of 1 M Na₂SO₄ aqueous solution under different compressive stresses and a scan rate of 50 mV/s. Under the action of large compressive stresses of 20.38 and 40.75 MPa, the CV curves exhibit quasi-rectangular shape, representing good capacitive characteristic. Under the action of compressive stresses less than or equal to 10.19 MPa, the CV curves deviate from the quasi-rectangular shape and change to slender profile with the decrease of the compressive stress. The area enclosed in the CV curve decreases with the decrease of the compressive stress, suggesting that increasing compressive stress can increase the energy storage

in the AC-sphere-based supercapacitors. Such behavior is similar to the trend reported by Li et al. [10] and Masarapu [11]. It needs to be pointed out that increasing the compressive stress generally can improve the electrochemical performance of supercapacitors by reducing the contact resistance and the travel distance of ions. However, an excessive compressive stress can cause the closure of open channels and pores and structural damage, leading to the decrease in the electrochemical performance, as observed by Gourdin et al. [9]. Thus, a proper level of compressive stress is needed to achieve a high power and a lower ESR.

Fig. 4b depicts the CV curves of the symmetrical supercapacitor cells under a compressive stress of 40.75 MPa and a scan rate of 50 mV/s for aqueous electrolytes of different Na₂SO₄ concentrations. For the CV curves of the symmetrical supercapacitor cells under other compressive stresses, see Fig. S1 in Supplementary Information. Under the compressive stress of 40.75 MPa, decreasing the Na₂SO₄ concentration in electrolyte leads to the shape change of the CV curve from the quasi-rectangle to the slender shape, suggesting that increasing ionic concentration can improve the energy storage in the AC-sphere-based supercapacitors. As shown in Fig. S1a, all the CV curves under the compressive stress of 2.55 MPa exhibit slender shape, indicating less-favored capacitive characteristic for all the electrolytes used in this work. Increasing the compressive stress results in the shape of the CV curves closely resembling a quasi-rectangle for the aqueous electrolytes with the Na₂SO₄ concentration being larger than or equal to 0.5 M. Note that decreasing the Na₂SO₄ concentration in electrolyte leads to the shape change of the CV curve from the quasi-rectangle to the slender shape. Such a trend suggests that increasing the ionic concentration can improve the energy storage in the AC-sphere-based supercapacitors.

Fig. 5a presents the GCD curves of the symmetrical supercapacitor cells at a current density of 2 A $\rm g^{-1}$ under different compression stresses for 1 M $\rm Na_2SO_4$ aqueous solution as electrolyte. All the GCD curves exhibit relatively symmetric-triangular profile, which suggests fast charging and discharging characteristics associated with the migration of ions in electric field. The IR drop decreases with the increase of the compressive stress, i.e. increasing the compressive stress reduces the energy loss associated with the decrease of the internal resistance of the supercapacitor cells.

Fig. 5b displays the GCD curves of the symmetrical supercapacitor cells at a current density of 2 A g^{-1} under a compressive stress of 40.75 MPa for aqueous electrolytes with different Na₂SO₄ concentrations. For the GCD curves of the symmetrical supercapacitor cells under other compressive stresses, see Fig. S2 in Supplementary Information. It is evident that increasing the Na₂SO₄ concentration and/or the compressive stress increases the regularity (i.e.

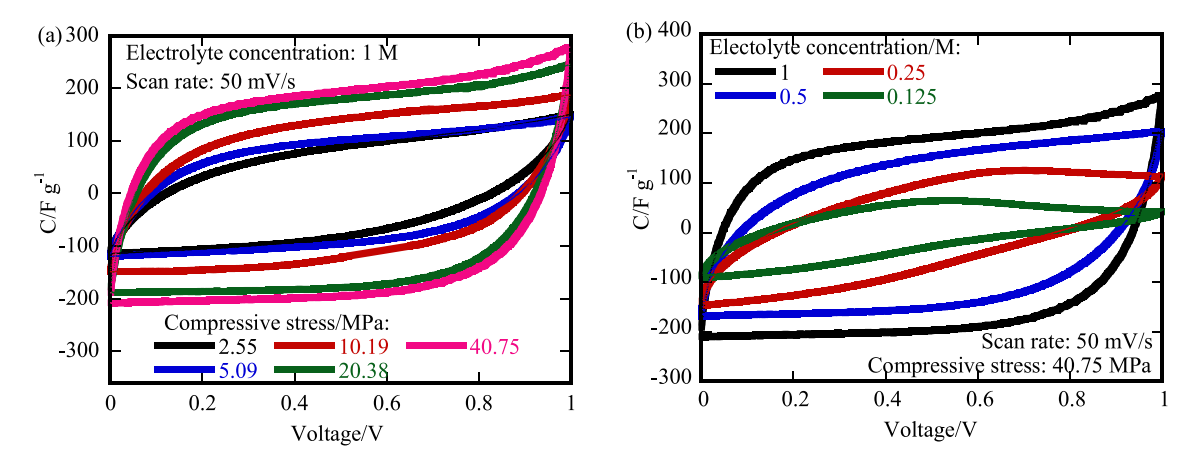


Fig. 4. CV curves of the symmetrical supercapacitor cells with 50 mV/s scan rate: (a) 1 M Na₂SO₄ aqueous solution under different compressive stresses, and (b) a compressive stress of 40.75 MPa for aqueous electrolytes of different Na₂SO₄ concentrations.

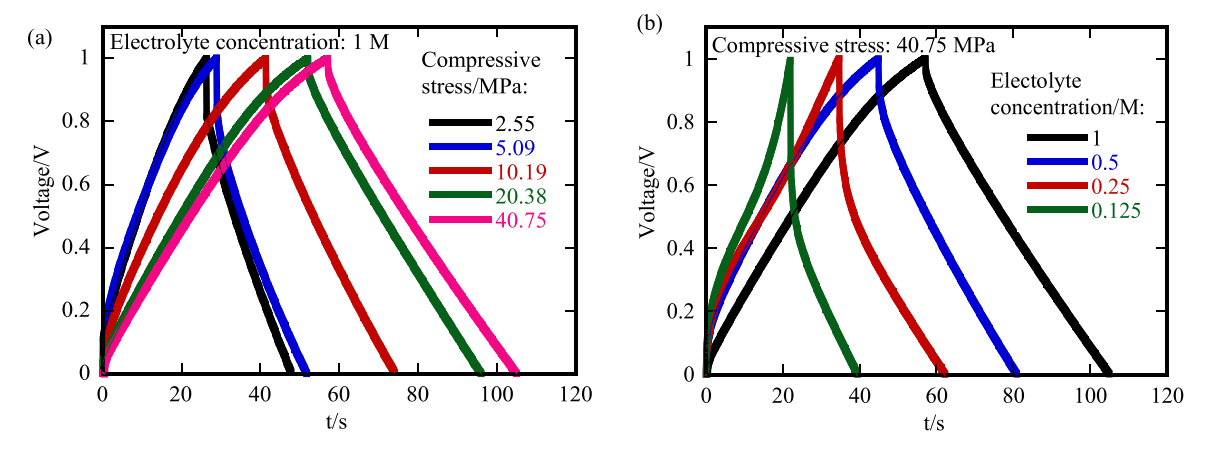


Fig. 5. GCD curves of the symmetrical supercapacitor cells at a current density of 2 A g^{-1} : (a) 1 M Na₂SO₄ aqueous solution under different compressive stresses, and (b) a compressive stress of 40.75 MPa for aqueous electrolytes of different Na₂SO₄ concentrations.

symmetry and linearity) of the GCD curves, suggesting the increase in the flux/accumulation of ions to/in the AC spheres. Notably, there exists dramatic decrease of the IR drop with the increase of the $\rm Na_2SO_4$ concentrations due to the increase in ionic conductivity associated with ionic concentration. In general, increasing the electrolyte concentration and/or the compressive stress increases the capacitive characteristics of the supercapacitor cells, which is qualitatively in good agreement with the behavior from the analysis of the CV curves.

The electrochemical impedance of the symmetrical supercapacitor cells was characterized in a frequency range of 0.01 Hz to 1 MHz under the condition of open circuit voltage. Fig. 6a-b displays the Nyquist plots of the symmetrical supercapacitor cells with 1 M Na₂SO₄ aqueous solution as electrolyte under different compression stresses and with aqueous electrolytes of different Na₂SO₄ concentrations under a compressive stress of 40.75 MPa, respectively. For the Nyquist plots of the symmetrical supercapacitor cells under other compressive stresses, see Figs. S3 and S4 in Supplementary Information. It is evident that there are three segments in the typical Nyquist plots, including a semi-circle in the high-frequency regime, a line-segment at an angle of ~45° with respect to horizontal axis in the intermediate-frequency regime, and a steep line-segment in the low-frequency region.

From the Nyquist plots, we can determine the series resistance, R_s , (a sum of the ionic resistance of electrolyte, intrinsic resistance of electrode materials, and contact resistances at interfaces between the electrolyte and the electrode and between the electrode and the current collector [21]) from the left intercept with

the horizontal axis. The series resistances are ~1.66, ~1.23, ~1.10, ~1.03 and ~0.97 Ω for the cells under the compressive stresses of 2.55, 5.09, 10.19, 23.28 and 40.75, respectively. Applying the compressive stress on the supercapacitor cells caused slight decrease of the series resistance. Also, the diameter of the semi-circle decreases with the increase of the compressive stress, indicating the decrease of the charge transfer resistance. The slope of the straight segment in the low-frequency regime increases with the increase of the compressive stress, suggesting the improvement of the capacitive behavior.

Under the action of 40.75 MPa, the Nyquist plots for all the supercapacitor cells exhibit the transition from the line segment corresponding to the regime of intermediate frequency to the one corresponding to the regime of low frequency (Fig. 6b). The slope of the line segment in the regime of low frequency increases with the increase of the Na₂SO₄ concentration in the aqueous electrolyte for the Na₂SO₄ concentration in the range of 0.25 to 1 M. Increasing the Na₂SO₄ concentration in the aqueous electrolyte caused the degeneration of the semi-circle in the regime of high frequency. The transition from the intermediate-frequency regime to the low-frequency regime with the increase of the ionic concentration and conductivity indicates the improvement in the capacitive behavior.

From to Fig. S3a in Supplementary Information, we note that there is no typical slope transition and "knee frequency" for the Nyquist plots of the supercapacitor cells with aqueous electrolytes of 0.25 M and 0.125 M of Na₂SO₄, which may be ascribed to the low conductivity. The Nyquist plot with the 0.125 M Na₂SO₄ aqueous solution as electrolyte exhibits the largest semi-circle in the

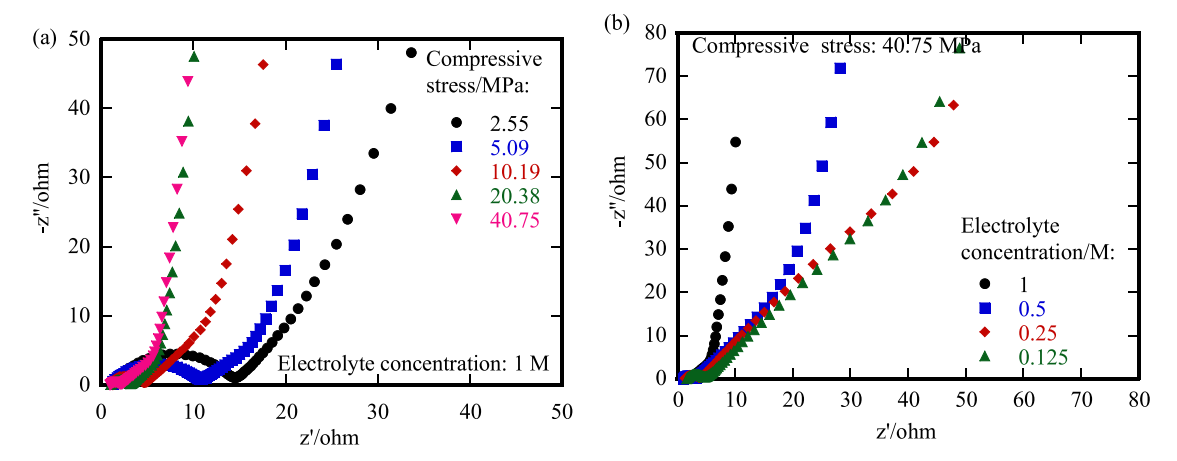


Fig. 6. Nyquist plots of the symmetrical supercapacitor cells: (a) 1 M Na₂SO₄ aqueous solution under different compressive stresses, and (b) a compressive stress of 40.75 MPa for aqueous electrolytes of different Na₂SO₄ concentrations.

high-frequency regime, suggesting the largest charge transfer resistance, which is due to the lowest ionic concentration and conductivity. For other electrolyte concentrations under small compressive stress, there is no significant difference in the high frequency regime, indicating limited effect of the electrolyte concentration on reducing the charge transfer resistance.

4. Discussion

Using Eq. (1) and the GCD curves for different current densities under different compressive stresses, we calculate the specific gravimetric capacitances of the symmetrical supercapacitor cells with the AC spheres as electrode material.

Fig. 7a-d shows the variation of the specific gravimetric capacitance with the compressive stress for different Na_2SO_4 concentrations in aqueous electrolyte under four different current densities of 1, 2, 5 and 10 A g^{-1} , respectively. It is evident that increasing the compressive stress and/or the Na_2SO_4 concentrations increases the specific gravimetric capacitance of the symmetrical capacitor cells under the same current density.

The increase of the specific gravimetric capacitance with the compressive stress is generally in consistence with the trend reported by Li et al. [3], Li et al. [10] and Masarapu et al. [11]. Masarapu et al. [11] in the study of the pressure effect on the electrochemical performance of flexible supercapacitors with nanostructured AC fibers as electrode material introduced an empirical relationship between the specific capacitance and the pressure (compressive stress) as

$$C = a \left[1 - f + fg(x) \left(1 - \left(\frac{P_0}{P} \right)^n \right) \right]$$
 (2)

in which a is a constant depending on the areal density of ions, f is the fraction of plane surface on the AC fibers covered by the pores, g(x) is a function depending on local surface topology of current collectors (average ratio of depth to width of cone-like surface cavities), P_0 is the atmospheric pressure, P is applied pressure, and $n \geq 2/3$ is a curve-fitting parameter. Eq. (2) is based on the dependence of the compaction of hydrated ions over the pore surface on applied pressure and geometric factors of local pore-surface without taking into account the change of local density/compaction associated with the decrease of electrode layer under pressure (compressive stress). From Eq. (2), we note that C approaches constant as $P \rightarrow \infty$. Such a trend is not in consistence with the results shown in Fig. 7a-c for the current densities of 1, 2 and 5 A g^{-1} , while the variation of the specific gravimetric capacitance with the compressive stress at the current density of 10 A g-1, as shown in

Fig. 7d, might follow the trend given in Eq. (2). The different trends in the variation of the specific capacitance with the compressive stress suggest that there likely exists electromechanical interaction, which determines the ionic migration and energy storage in the AC spheres, as well as the structural change in the AC spheres and current collectors induced by large compressive stress and large current density. It needs to be pointed that the constant capacitance from Eq. (2) for $P \rightarrow \infty$, which depends on the initial surface topology of current collectors, cannot explain the results given by Gourdin et al. [9], since the results given by Gourdin et al. [9] reveal the thickness dependence of the saturated capacitance. Note that the double-layer capacitance is dependent on the geometric shape of pores [22]. An elliptical pore can store more ions than a cylindrical pore of the same cross-sectional area and length, since the elliptical pore of the same cross-section area possesses a larger surface area than the cylindrical pore.

According to Fig. 7a-c, we can express the dependence of the specific capacitance on the compressive stress for the current density in the range of 1 to 5 A g^{-1} as

$$C = C_0 \sigma^m \text{ for } 2.55 \le \sigma \le 40.75$$
 (3)

where σ is the compressive stress acting on the current collector in the unit of MPa, and C_0 and m are two fitting constants. Here, C_0 in the unit of F/g can be approximated as the specific gravimetric capacitance under a compressive stress of 1 MPa, i.e. σ =1 MPa. Note that the limitation of the load cell used in the compression machine cannot maintain a stable, compressive stress of 1 MPa. No electrochemical characterization under compressive stress less than 2.55 MPa was performed.

Using Eq. (3) to curve-fit the data in Fig. 7a-c, we obtain the parameters of C_0 and m. For comparison, the fitting curves are also included in the corresponding figures. It is evident that Eq. (3) can be used to correlate the specific gravimetric capacitance of the symmetric supercapacitor cells made from the AC spheres for the compressive stresses in the range of 2.55 to 40.75 MPa and the current density in the range of 1 to 5 A g^{-1} .

Fig. 8a-b illustrates the variations of the parameters of C_0 and m with the Na_2SO_4 concentration for different current densities, respectively. It is evident that both the C_0 and m are dependent on the current density. The larger the current density, the smaller is the C_0 , and the larger is m. Under the same current density, the C_0 increases generally with the increase of the Na_2SO_4 concentration. For the current densities of 1 and 2 A g^{-1} , the increasing rate of the C_0 is relatively small, and the C_0 can be approximated as constants of 99.4 ± 3.7 and 83.8 ± 4.9 , respectively. For the current density of $5 A g^{-1}$, the C_0 is in the range of 30.8 to 56.2, suggesting

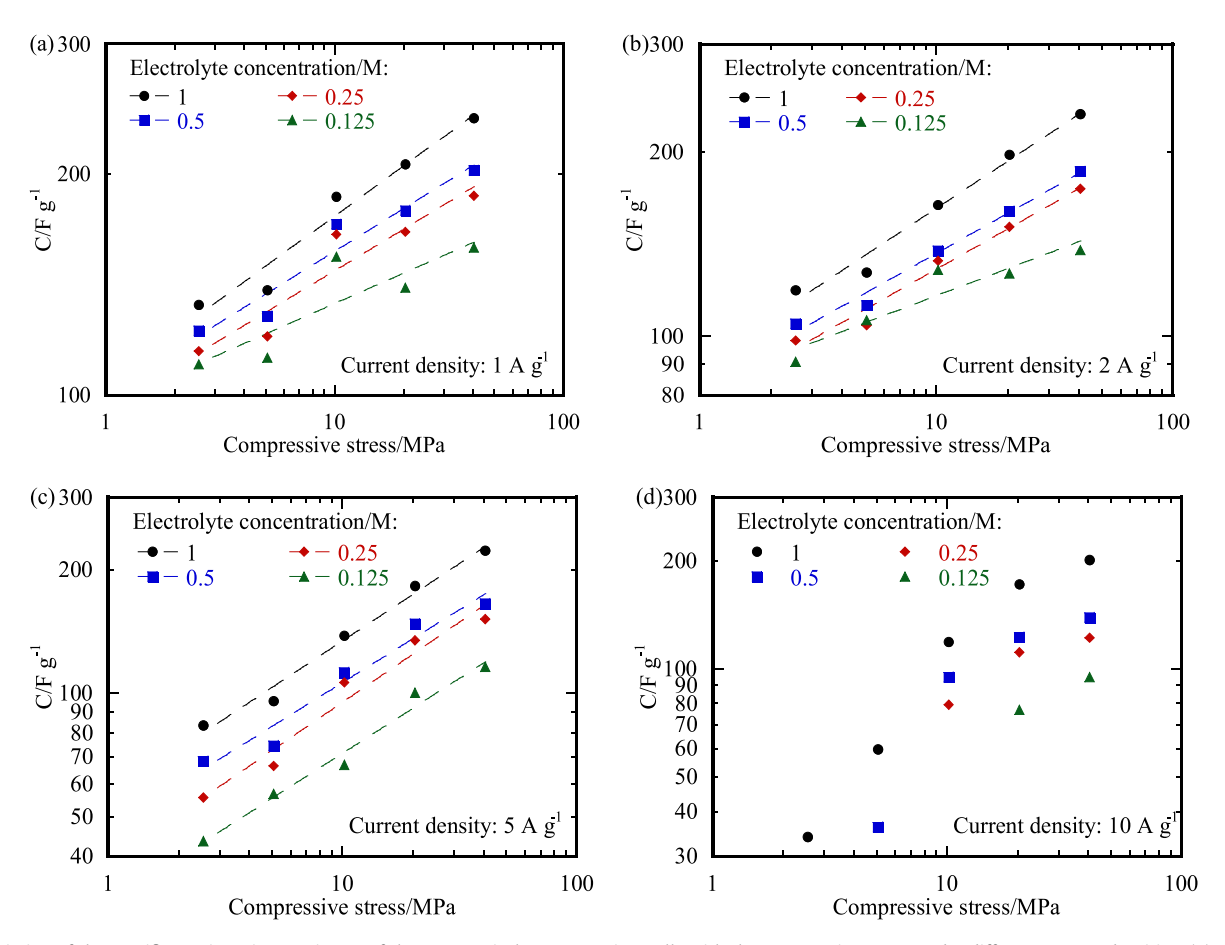


Fig. 7. Variation of the specific gravimetric capacitance of the symmetrical supercapacitor cells with the compressive stress under different current densities: (a) 1 A g^{-1} , (b) 2 A g^{-1} , (c) 5 A g^{-1} , and (b) 10 A g^{-1} .

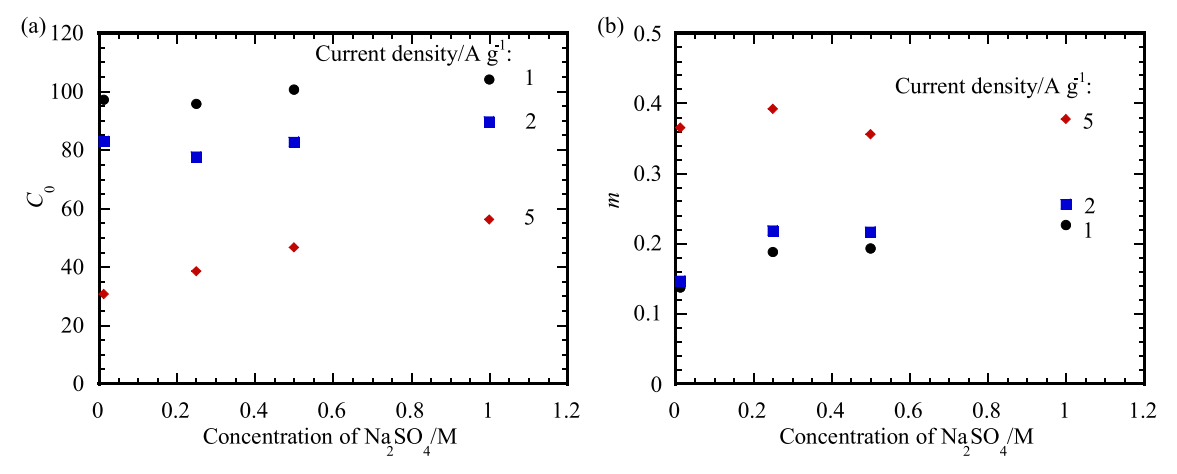


Fig. 8. Variations of the parameters of C_0 and m with the Na_2SO_4 concentration for different current densities: (a) C_0 , and (b) m.

the relatively strong effect of the Na_2SO_4 concentration. The variation of the parameter m with the Na_2SO_4 concentration under the same current density is relatively small and can be approximated as constants of 0.19 ± 0.04 , 0.21 ± 0.05 and 0.37 ± 0.02 , respectively for the current densities of 1, 2 and 5 A g^{-1} .

There are various factors controlling the energy storage in AC-based supercapacitors, including ionic size, electrolyte concentration, temperature, electrode thickness and microstructure/topology of ACs. Under mechanical loading, ACs can experience mechanical deformation, as revealed by the nanoindentation of carbon spheres [23,24]. We expect that the compressive stress applied on the cur-

rent collector caused the deformation of the PTFE powder and AC spheres, leading to the decrease in the electrode thickness (compaction of the electrode materials) and the change in the porosity/pore sizes. The decrease in the electrode thickness reduces the travel distance of ions into the electrode, which benefits for the fast charging and discharging and causes the decrease of the internal resistance. It needs to be pointed out that applying compressive stress can cause the change of pore shapes, such as from a cylindrical pore to an elliptical pore, and the closure of pores. Under a small compressive stress, it is expected that there is no closure of pores and the surface area of the pores increases. Under a

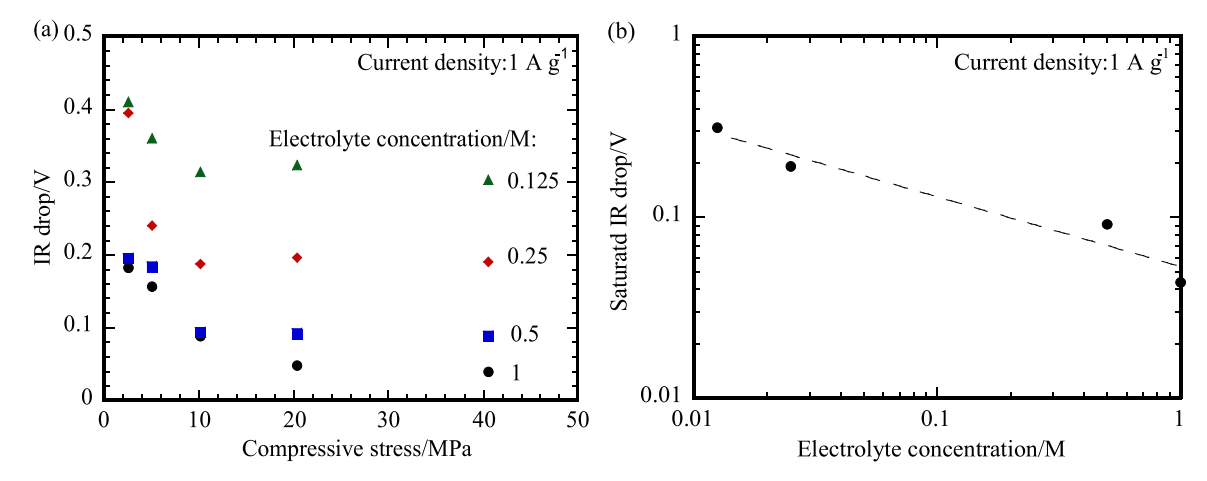


Fig. 9. (a) Variation of the IR drop with compressive stress at a current density of 1 A g⁻¹, and (b) variation of the saturated IR drop with the electrolyte concentration.

large compressive stress, closure of pores can occur, likely leading to the decrease of the surface area and capacitance.

Detsi et al. [25] performed dimensional analysis and obtained the following relationship for a nanoporous material with an average pore size of d_0 , a total surface area, S_0 , and an average density ρ_0

$$S_0 \propto \phi_0(\rho_0 d_0)^{-1} \tag{4}$$

in which ϕ_0 is the porosity of the nanoporous material. Assume that the electrode can be approximated as a disc of h_0 in thickness and r_0 in radius with an average density of ρ_0 , at initially "stressfree" state. Under the action of a compressive stress, σ , the thickness of the electrode reduces to h. The density of the electrode, ρ , becomes

$$\rho = \rho_0 \frac{h}{h_0} \tag{5}$$

Note that Eq. (5) is valid under the condition that the change of the radius of the disc is negligible. Using Eqs. (4) and (5), we obtain the total surface area of the electrode, *S*, which experiences the thickness change under a compressive stress, as

$$\frac{S}{S_0} = \frac{\phi d_0}{\phi_0 d} \cdot \frac{\rho_0}{\rho} = \frac{\phi d_0}{\phi_0 d} \cdot \frac{h_0}{h} = \frac{\phi d_0}{\phi_0 d} \cdot \left(1 - \frac{h_0 - h}{h_0}\right)^{-1} \tag{6}$$

in which $(h_0-h)/h_0$ is the compressive strain. For plastic deformation under uniaxial loading, plastic strain is a power law function of applied stress, i.e. plastic strain \propto (applied stress) $^{\alpha}$ with α being a power index. Using the power-law relation in Eq. (6), we have

$$\frac{S}{S_0} = \frac{\phi d_0}{\phi_0 d} \cdot \frac{1}{1 - \lambda \sigma^{\alpha}} \approx \frac{\phi d_0}{\phi_0 d} (1 + \lambda \sigma^{\alpha}) \tag{7}$$

for $\lambda\sigma^{\alpha}<<1$. Note that there is $0<(h_0-h)/h_0<1$. It is evident that the total surface area of the electrode made from porous ACs increases generally with the increase of the compressive stress if the ratio of the ϕ/d remains relatively unchanged and there is no closure of pores. Increasing the total surface area leads to the increase of the active sites available for the accumulation of ions on the surfaces of the pores and AC spheres. Note that a large compressive stress can cause the closure of pores, likely leading to the decrease of the surface area and the increase of the conductivity.

According to Sun et al. [26], the specific areal capacitance is a linear function of the areal fractions of micropores and mesopores. The specific gravimetric capacitance is generally proportional to the specific areal capacitance. Therefore, we have

$$C = \kappa \frac{\phi d_0 S_0}{\phi_0 d} (1 + \lambda \sigma^{\alpha}) = \chi (1 + \lambda \sigma^{\alpha})$$
(8)

with κ and χ being two proportionality constants. Eq. (8) reveals the stress dependence of the specific gravimetric capacitance, which is qualitatively in agreement with the results shown in Fig. 7 and Eq. (3).

Fig. 9a shows the variation of the IR drop with the compressive stress at the current density of 1 A g^{-1} . It is evident that there are two regions for the variation of the IR drop with the compressive stress; one corresponds to rapid decrease of the IR drop for the compressive stress in the range of 2.55 to 10.19 MPa, and the other corresponds to a plateau region with nearly constant IR drop for the compressive stress in the range of 20. 38 to 40.57 MPa. The rapid decrease of the IR drop can be attributed to the increase in the contact between the electrode materials and the current collector. In the plateau region, increasing the compressive stress did not result in significant decrease of the IR drop, which is likely due to the presence of compression-induced local cracks similar to the cracking in concrete under compression [27].

It is known that the contact resistance, *R*, for the contact between solid surfaces as a function of the contact load, *F*, is [28]

$$R = \xi F^{-1/2} \tag{9}$$

where ξ is a constant depending true contact area. The decreasing trend of the IR drop shown in Fig. 9 is qualitatively in agreement with Eq. (9). However, the electrical conduction in a supercapacitor cell is much more complicated than the electrical conduction in solid and involves ionic conduction. Eq. (9) cannot reveal all the mechanisms involving in the compression-induced decrease of the internal resistance (IR drop).

Using the IR drops in the plateau region, we calculate the average IR drop and define the average IR drop as the saturated IR drop. Fig. 9b depicts the dependence of the saturated IR drop on the electrolyte concentration. It is evident that the saturated IR drop, $IR_{\rm S}$, is a power function of the electrolyte concentration, φ , as

$$IR_{S} = \beta \varphi^{b} \tag{10}$$

where β and b are fitting parameters. Using Eq. (10) to curve-fit the results in Fig. 9b, we obtain b=-0.39.

From the line segment of ~1 in slope in the regime of intermediate frequency of the Nyquist plot, we can calculate the nominal diffusion coefficient of ions, *D*, in the AC spheres in the symmetrical supercapacitor cells as [29,30]

$$D = \frac{R_g^2 T^2}{2An_i^4 F_F^4 C_i^2 \sigma_w^2} \tag{11}$$

where R_g is the gas constant, T is absolute temperature (298.15 K), A is the nominal area of the electrode (19.63 mm²), n_i is the charge

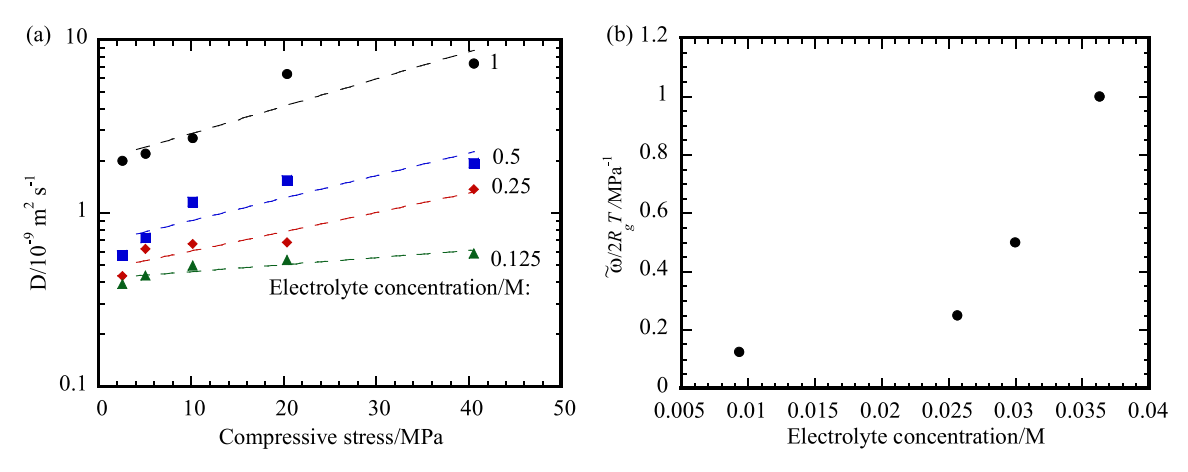


Fig. 10. (a) Variation of the nominal diffusion coefficient with the compressive stress for different electrolyte concentration, and (b) dependence of the parameter ω on the electrolyte concentration.

of electrolyte ions, F_F is the Faraday constant, and C_i is ionic concentration in electrolyte. The Warburg factor, σ_w , is the slope of z' v.s. $\omega^{-0.5}$ (ω is frequency). In the calculation of σ_w , we used the end point of the semi-circle as the first point and the point corresponding to the transition from the regime of intermediate frequency to the regime of low frequency as the last point from the Nyquist plot.

Fig. 10 displays the variation of the nominal diffusion coefficient with the compressive stress for different electrolyte concentrations. It is evident that the nominal diffusion increases with the increase of the compressive stress and the $\rm Na_2SO_4$ concentration in the aqueous electrolyte.

It is known that diffusion coefficient is proportional to the jump frequency of the diffusing species. According to the theory of thermal activation process [31,32], the jump frequency is dependent on temperature and mechanical stress. The diffusion coefficient as a function of mechanical stress is

$$D = D_0 e^{-(Q - \tau \varpi)/R_g T} \tag{12}$$

where D_0 is a pre-exponential factor, Q is the activation energy for the rate process, τ is shear stress, and ϖ is the activation shear volume. Under uniaxial compression, $\tau = \sigma/2$. Using Eq. (12) to curvefit the results in Fig. 10a, we obtain $\varpi/2R_gT$. For comparison, the fitting curves are included in Fig. 10. In general, Eq. (12) can describe well the stress-dependence of the ionic diffusion coefficients. There exists stress-assisted diffusion of ions in the AC spheres during electrochemical cycling.

Fig. 10b depicts the dependence of $\varpi/2R_gT$ on the electrolyte concentration. It is interesting to note that the parameter of $\varpi/2R_gT$ increases with the increase of the Na₂SO₄ concentration in the aqueous electrolyte. Such a result suggests that increasing the Na₂SO₄ concentration increases the activation shear volume and reduces the energy barrier needed for the ionic migration in electrochemical environment under compressive stress.

5. Summary

In summary, we have investigated the effects of compressive stress on the electrochemical performance of the symmetrical supercapacitor cells, which were made from AC spheres, for different Na_2SO_4 concentrations in the electrolyte under different current densities. The AC spheres were synthesized from xylose via the combination of three steps: hydrothermal carbonization, carbonization at 500 °C in nitrogen environment and chemical activation with KOH at 800 °C in nitrogen environment. The following summaries the main results obtained in this work.

- 1 The carbonization of the solid product from the hydrothermal carbonization of xylose at 500 °C in nitrogen environment helps maintain the geometrical topology of the solid product after the chemical activation with KOH at 800 °C, i.e. the activated-carbon particles maintain the spherical shape of the xylose-derived carbon particles from the hydrothermal carbonization.
- 2 Applying compressive stress onto the current collector leads to the compaction of the electrode materials, which reduces the thickness of the electrode and increases the total surface area of the electrode materials for the compressive stresses used in this work.
- 3 A simple relation between the specific gravimetric capacitance and the compressive stress, which is qualitatively in agreement with the experimental results, has been derived from the framework of mechanical deformation, provided that there is no closure of pores under compressive stress.
- 4 The specific gravimetric capacitance is an increasing power function of the compressive stress for the current density less than or equal to 5 A g^{-1} , and the power indexes are 0.19 \pm 0.04, 0.21 \pm 0.05 and 0.37 \pm 0.02, respectively, for the current densities of 1, 2 and 5 A g^{-1} .
- 5 There are two regions for the variation of the IR drop with the compressive stress; one corresponds to rapid decrease of the IR drop, and the other corresponds to a plateau region with nearly constant IR drop.
- 6 There exists stress-assisted diffusion of ions in the AC spheres during electrochemical cycling. The nominal diffusion coefficient for the diffusion of ions in the AC spheres is an increasing, exponential function of the compressive stress.

Declaration of Competing Interest

The authors declare that they have no known competing financial interests or personal relationships that could have appeared to influence the work reported in this paper.

Acknowledgements

WS is grateful for the support from the National Natural Science Foundation of China (No. 21805123), the LiaoNing Revitalization Talents Program (XLYC1907067) and talent scientific research fund of LSHU (No.2016XJJ-077). FY is grateful for the support from the NSF (CMMI-1634540), monitored by Dr. Khershed Cooper.

Authorship Contribution Statement

Wei Sun: Experiment, Data curation, Writing - original draft.

Yulin Zhang: Experiment, Data curation.

Fuqian Yang: Conceptualization, Experimental design, Writing - review & editing, Supervision.

Supplementary materials

Supplementary material associated with this article can be found, in the online version, at doi:10.1016/j.electacta.2020.136874.

References

- [1] D.N. Futaba, K. Hata, T. Yamada, T. Hiraoka, Y. Hayamizu, Y. Kakudate, O. Tanaike, H. Hatori, M. Yumura, S. Iijima, Shape-engineerable and highly densely packed single-walled carbon nanotubes and their application as super-capacitor electrodes, Nat Mater 5 (2006) 987–994.
- [2] L. Hu, M. Pasta, F. La Mantia, L. Cui, S. Jeong, H.D. Deshazer, J.W. Choi, S.M. Han, Y. Cui, Stretchable, porous, and conductive energy textiles, Nano Lett. 10 (2010) 708–714
- [3] X. Li, J. Rong, B. Wei, Electrochemical behavior of single-walled carbon nanotube supercapacitors under compressive stress, ACS Nano 4 (2010) 6039–6049.
- [4] J.R. Miller, P. Simon, Electrochemical capacitors for energy management, Science 321 (2008) 651–652.
- [5] G. Wang, L. Zhang, J. Zhang, A review of electrode materials for electrochemical supercapacitors, Chem Soc Rev 41 (2012) 797–828.
- [6] R. Yuksel, B. Yarar Kaplan, E. Bicer, A. Yurum, S. Alkan Gursel, H.E. Unalan, All-carbon hybrids for high performance supercapacitors, Inter J Energy Res 42 (2018) 3575–3587.
- [7] M. Farhadi, O. Mohammed, Energy storage technologies for high-power applications, IEEE Trans Ind Appl 52 (2016) 1953–1961.
- [8] C. Portet, P.L. Taberna, P. Simon, E. Flahaut, C. Laberty-Robert, High power density electrodes for carbon supercapacitor applications, Electrochim. Acta 50 (2005) 4174–4181.
- [9] G. Gourdin, A. Meehan, T. Jiang, P. Smith, D.Y. Qu, Investigation of the impact of stacking pressure on a double-layer supercapacitor, J Power Sources 196 (2011) 523–529.
- [10] K.-B. Li, D.-W. Shi, Z.-Y. Cai, G.-L. Zhang, Q.-A. Huang, D. Liu, C.-P. Yang, Studies on the equivalent serial resistance of carbon supercapacitor, Electrochim. Acta 174 (2015) 596–600.
- [11] C. Masarapu, L.P. Wang, X. Li, B. Wei, Tailoring electrode/electrolyte interfacial properties in flexible supercapacitors by applying pressure, Adv Energy Mater 2 (2012) 546–552.
- [12] R. Zhang, Y. Xu, D. Harrison, J. Fyson, A study of the electrochemical performance of strip supercapacitors under static and dynamic mechanical tests, Inter J Electrochem Sci 12 (2017) 1463–1473.
- [13] R. Jia, H. Du, X. Zhang, Z. Chen, D. Chen, Stretchable and compressible supercapacitor with polyaniline on hydrogel electrolyte, J Electrochem Soc 165 (2018) A3792–A3798.

- [14] W. Sun, Y.L. Zhang, Z.X. Yang, F.Q. Yang, High-performance activated carbons for electrochemical double layer capacitors: effects of morphology and porous structures, Inter J Energy Res 44 (2020) 1930–1950.
- [15] M. Li, C. Liu, H. Cao, H. Zhao, Y. Zhang, Z. Fan, Koh self-templating synthesis of three-dimensional hierarchical porous carbon materials for high performance supercapacitors, J Mater Chem A 2 (2014) 14844–14851.
 [16] K. Wang, N. Zhao, S. Lei, R. Yan, X. Tian, J. Wang, Y. Song, D. Xu, Q. Guo, L. Liu,
- [16] K. Wang, N. Zhao, S. Lei, R. Yan, X. Tian, J. Wang, Y. Song, D. Xu, Q. Guo, L. Liu, Promising biomass-based activated carbons derived from willow catkins for high performance supercapacitors, Electrochim. Acta 166 (2015) 1–11.
- [17] W. Qian, F. Sun, Y. Xu, L. Qiu, C. Liu, S. Wang, F. Yan, Human hair-derived carbon flakes for electrochemical supercapacitors, Energy Environ Sci 7 (2014) 379–386.
- [18] L. Sun, C. Tian, M. Li, X. Meng, L. Wang, R. Wang, J. Yin, H. Fu, From coconut shell to porous graphene-like nanosheets for high-power supercapacitors, J Mater Chem A 1 (2013) 6462–6470.
- [19] M. Thommes, K. Kaneko, A.V. Neimark, J.P. Olivier, F. Rodriguez-Reinoso, J. Rouquerol, K.S. Sing, Physisorption of gases, with special reference to the evaluation of surface area and pore size distribution (iupac technical report), Pure Appl Chem 87 (2015) 1051–1069.
- [20] D.Y. Chung, K.J. Lee, S.H. Yu, M. Kim, S.Y. Lee, O.H. Kim, H.J. Park, Y.E. Sung, Alveoli-inspired facile transport structure of n-doped porous carbon for electrochemical energy applications, Adv Energy Mater 5 (2015) 1401309.
- [21] J. Luo, H.D. Jang, J. Huang, Effect of sheet morphology on the scalability of graphene-based ultracapacitors, ACS Nano 7 (2013) 1464–1471.
- [22] W. Zhou, F.Q. Yang, Integral capacitance of diffusion layer for rectangular structures, J Energy Storage 30 (2020) 101477.
- [23] Y. Sun, R. Chen, S.M. Lipka, F. Yang, Current-induced strength degradation of activated carbon spheres in carbon supercapacitors, Mater Res Express 3 (2016) 055602.
- [24] Y. Sun, R. Chen, G. Zhao, F. Yang, Nanoindentation of carbon microspheres, Inter J Mater Res 107 (2016) 687–691.
- [25] E. Detsi, E. De Jong, A. Zinchenko, Z. Vuković, I. Vuković, S. Punzhin, K. Loos, G. Ten Brinke, H. De Raedt, P. Onck, On the specific surface area of nanoporous materials, Acta Mater 59 (2011) 7488–7497.
- [26] W. Sun, S.M. Lipka, C. Swartz, D. Williams, F. Yang, Hemp-derived activated carbons for supercapacitors, Carbon 103 (2016) 181–192.
- [27] K.M. Nemati, P.J. Monteiro, K.L. Scrivener, Analysis of compressive stress-induced cracks in concrete, ACI Mater J 95 (1998) 617–630.
- [28] S. Timsit, Electrical contact resistance: properties of stationary interfaces, Proceedings of the Forty-Fourth IEEE Holm Conference on Electrical Contacts (Cat. No. 98CB36238), IEEE (1998) 1–19.
- [29] V.F. Lvovich, Impedance spectroscopy: Applications to Electrochemical and Dielectric Phenomena, John Wiley & Sons, 2012.
- [30] W. Sun, Y. Xiao, Q. Ren, F. Yang, Soybean-waste-derived activated porous carbons for electrochemical-double-layer supercapacitors: effects of processing parameters, J Energy Storage 27 (2020) 101070.
- [31] H. Eyring, Viscosity, plasticity, and diffusion as examples of absolute reaction rates, J Chem Phys 4 (1936) 283–291.
- [32] F. Yang, Field-limited migration of li-ions in li-ion battery, ECS Electrochem Lett 4 (2015) A7–A9.